SECED 2023 Conference
Earthquake Engineering & Dynamics for a Sustainable Future
14-15 September 2023, Cambridge, UK

FRAGILITY ASSESSMENT OF CONFINED MASONRY BUILDINGS EXPOSED TO SEQUENTIAL FLOOD AND SEISMIC HAZARDS

Ahsana PARAMMAL VATTERI[1] & Dina D'AYALA[2]

Abstract: *Multiple hazards affecting a region produce cascading or consequential effects, depending on the space and time windows in which they act. Recurring floods of moderate intensities in a region with high exposure to flood and seismic hazards, may not cause major structural damage, although they produce saturation and material degradation in the lower courses of masonry walls. Such degradation, usually not repaired, accumulates over the years. Therefore, if an earthquake of given intensity strikes during a flood season, the damage caused is the result of the concurrent effect of seismic acceleration, the material degradation and flood loads. In order to capture these combined effects in the fragility functions, a loading regime is devised in this paper that imposes, on the building with reduced material capacities in the lower courses, first the hydrostatic pressure representing the intensity of selected incremental flood depths, followed by the ground acceleration, increasing until the failure of the building. Selected confined masonry school buildings are modelled and analysed with this loading scheme using a platform based on Applied Element Method, to derive the capacity curves. Fragility functions are then derived for the combined load cases, for each increment of flood depth, following the N2 method. The paper presents two-dimensional fragility functions that characterise the physical fragility of the buildings corresponding to five flood depths followed by seismic action. These functions allow to define the probability of the state of damage of individual buildings, conditioned to the joint probability of a given PGA and a given flood depth, which is useful for probabilistic assessment at the inventory as well as the system level.*

Introduction

Increasing imbalance in the environmental systems due to rapid urbanisation and climate change tends to aggravate the likelihood of multiple natural hazards, acting in the most vulnerable geographic locations. As many countries are exposed to more than one hazard (Dilley et al. 2005), it is particularly important to assess the vulnerability of buildings with critical functions such as schools, against multiple hazards. Multi-hazard scenarios can be understood as one of the following (Gehl, 2017): simultaneous events (different hazard occurring in the same space and time window), cascading events (one hazard triggering another hazard), consequential events (when effects of the hazards are cascading) and dependent events (when occurrence of one event influences the probability of occurrence of another). The necessity of shifting from single hazard risk to multi-hazard risk is highlighted by recent studies (D'Ayala *et al.*, 2006, 2016; Gallina et al. 2016; Bruneau et al. 2017; de Ruiter et al. 2020b, a) and international initiatives such as the Johannesburg Plan in 2002 (UN, 2002), Hyogo Framework for action (ISDR, 2005), and more recently, the Sendai framework (UNISDR, 2015), which incorporated the multi-hazard approach into the guiding principles of 2015-2030 agenda. As a result, frameworks for the hazard interaction are being developed for the holistic resilience assessment of engineering systems (Marzocchi *et al.*, 2012; De Angeli *et al.*, 2022).

Earthquakes and floods are two major life-threatening and destructive hazards in the context of schools as evidenced from past events. There exist significant overlap of regions exposed to both these hazards (Ritchie and Roser, 2014), making a combined-hazard vulnerability assessment of school buildings particularly relevant. A few studies have examined specific combination of seismic and flood risk in the context of disaster risk reduction of general class of buildings (for example Dabbeek et al. 2020; Murnane et al. 2017; Shah et al. 2018), however, assessment of their combined effects on buildings in general and school infrastructure systems specifically, are not known to the authors. Hence, in addition to the effects of individual hazards, the combined effects of flood with seismic action is an area requiring further research, especially considering the asynergies in the risk assessment in relation to these hazards (de Ruiter *et al.*, 2017; de

[1] Dr, UCL, London, UK, ahsana.vatteri.17@ucl.ac.uk
[2] Prof, UCL, London, UK

Ruiter, de Bruijn, *et al.*, 2020). One of the reasons for limited advancement in the field of combined hazards vulnerability assessment, is the requirement for fragility models based on joint loading from different hazards, corresponding to the cascading or sequential nature of the hazards (Marzocchi *et al.*, 2012). The state of development and techniques of individual hazard vulnerability assessment vary between different hazards (Putrino, 2021), which represents a challenge in defining a homogeneous approach in defining combined hazard setting. A third aspect of complexity is the measure of vulnerability in the context of different hazards. For instance, seismic vulnerability assessments are often dominated by structural aspects of the infrastructure, while flood vulnerability accounts more for the disruption of social and functional aspects (de Ruiter *et al.*, 2017). Probability-based approaches and artificial intelligence tools are recommended to address the complexities of multi-hazard analysis and design of structures and systems (Roy and Matsagar, 2021).

This paper examines the combined effects of floods and earthquakes on the performance of school buildings, as they are crucial for the disaster risk reduction of communities. Disruption from hazards to school education systems is a growing concern, as evidenced by several global endeavours (GPSS, 2014; UNISDR, 2015; The World Bank, 2019; GADRRRES, 2022) to understand and reduce the vulnerability of schools. In regions of high exposure, yearly flood events weaken school buildings, especially masonry buildings, rendering them more vulnerable to subsequent earthquake shaking, which may or may not coincide with a flood season. This paper presents a methodology for analysing the sequential effects of floods followed by an earthquake, resulting in analytical multi-hazard fragility functions of masonry school buildings.

Methodology

Fragility functions are widely used for probabilistic seismic vulnerability assessment of structures (Calvi *et al.*, 2006). Analytical fragility functions expressing likelihood of damage against levels of hazard intensity are a suitable choice to represent fragility of buildings in the absence of empirical data (Rossetto and Elnashai, (2003). In this study, analytical fragility assessment involving numerical modelling and seismic analysis of buildings (D'Ayala *et al.*, 2015) is expanded to combined flood-seismic analysis for the performance assessment of selected school buildings. The methodology for this assessment is explained in this section and illustrated in Figure 1.

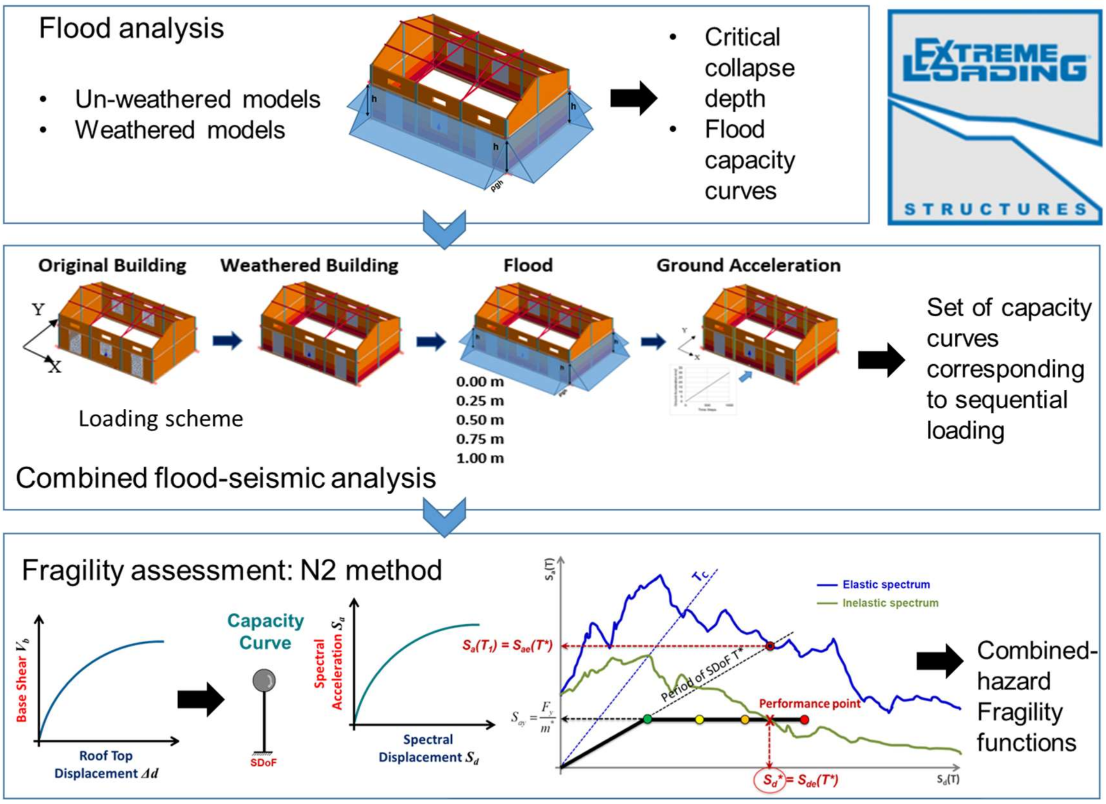

Figure 1. Summary of the methodology of this paper

Simulation of flood loading:

It is assumed that any structure in a flood plane would have been exposed to several flood events in their lifetime, which would have weakened the mechanical integrity of the lower courses of the masonry walls. Therefore, if an earthquake strikes during a flood season, the damage caused is the result of the concurrent effects of the material degradation, the flood loads and the seismic acceleration. However, it is necessary to quantify the depth of flood that would cause collapse of the considered structure, i.e. its flood capacity, before investigating the sequential effect of a subsequent earthquake. Hence, an incremental flood analysis is first performed by assuming the hydrostatic component of flood water. A combined loading scheme in accordance with the expected flood hazard levels of the location of interest is then designed, to address the combined flood-seismic hazard scenario, as shown in Figure 1. Hydrostatic flood loads corresponding to specified depth are applied to the structure with weathered material properties, followed by an incremental ground acceleration up to failure. With reference to the 100 years maximum expected flood, the sequential loading is repeated for different increments of the water depths, to derive the capacity curves associated with different flood magnitudes.

Capacity assessment:

The flood and combined flood-seismic loading schemes described above are implemented for capacity assessment through numerical modelling and analysis of selected school buildings on Extreme Loading for Structures (ASI, 2018), which is a specialist software based on Applied Element Method (AEM). ELS has in-built capability of hydrostatic loading, representing slow-rising stagnant flood water, and advanced non-linear seismic analysis. The degradation of the buildings from repeated historic flooding is incorporated in the models through weathered material properties in the lower part of the building, adopted from the experimental investigations in the literature. The hydrostatic pressure is applied on the exterior of all the walls, simulating the worst condition of lateral load imbalance. Seismic action is simulated by monotonously increasing Ground Acceleration (GA) instead of an explicit lateral force or displacement, as this technique of applying GA for non-linear static pushover analysis overcomes the difficulty of such analysis on buildings with flexible diaphragms. Detailed description of this seismic analysis procedure can be found in Adhikari *et al.*, (2023). The resulting capacity curve provides the evolution of a chosen engineering demand parameter (EDP) with increasing intensity measure (IM) of the ground motion.

Fragility assessment:

Fragility functions convert the capacity curves obtained from numerical analysis to probability of exceeding specified damage states or performance thresholds, across a range of hazard intensities. This involves the estimation of performance points (IM-EDP points) by comparison of the seismic capacity to demand, and fitting a probabilistic function to the cloud of IM-EDP points, very often a cumulative lognormal distribution, using statistical regression approaches (Gehl, 2017). The N2 method (Fajfar, 2000), is applied by using the idealised SDOF capacity curves from a non-linear static pushover analysis against natural response spectra in the acceleration-displacement response spectral space (ADRS) to identify performance points as coordinates of IM and EDP.

Two representative confined masonry school buildings varying in the seismic design level are chosen from a sample of schools in Guwahati, India, a region affected by recurring flooding and of highest seismicity in India. These are masonry buildings with flexible diaphragms, and variable level of confinement of the masonry panels by means of reinforced concrete elements, hence categorised as poor design (PD) level and medium design (MD) levels. While the PD structure has poor connections and minimal horizontal confinement (plinth and lintel band), the MD structure has good connections and horizontal bands at plinth, sill, lintel and roof. Both have vertical confining columns at regular intervals and corners. Better confinement and connection between the masonry and confinement are expected to result in better seismic performance. A complete description of this classification system with the details of the criteria defining the seismic design levels, and the specific features of these school buildings can be found in Parammal Vatteri and D'Ayala (2021).

Flood capacity assessment

The building models are exposed to the hydrostatic loads from increasing flood depths until a definite partial or total collapse is observed, which is defined by a large increase in displacement for a small increment of water depth. The loading scenario (Figure 2) assumes that the buildings are surrounded by floodwater on all four sides, and there is no considerable ingress of water to the inside. Although this is not necessarily the most realistic scenario, as there might be ingress of water and therefore some extent of balancing of internal and external hydrostatic pressure, it represents an extreme case of unbalanced lateral loading on the walls and therefore useful to define the vulnerability to the extreme conditions (Mendis *et al.*, 2014). Effects of flow velocity and hydrodynamic effects are not considered at this stage, although this can be included by equivalent static conversion. This is because fluvial and pluvial flooding are usually static in nature, with very low velocity (Nofal and van de Lindt, 2020), causing damage in structures mainly due to flood depth and duration, although flash flooding is also becoming a more common hazard.

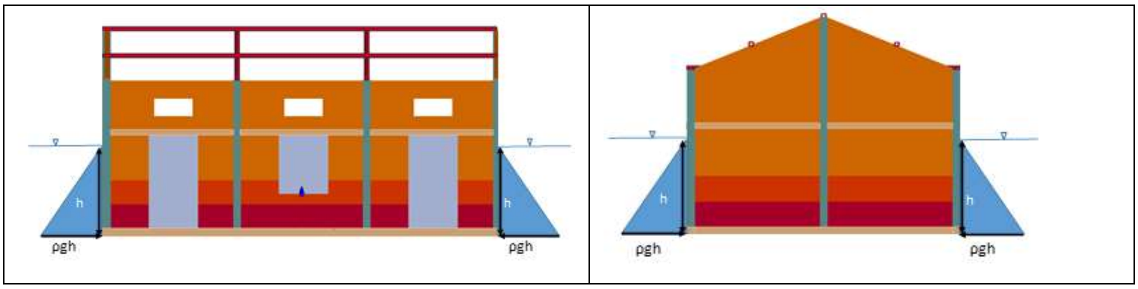

Figure 2. Flood loading pattern on weathered building models

In order to study the influence of material degradation due to several years of flooding, two sets of models are analysed under flood loading, namely un-weathered and weathered models. Considering that the maximum depth of flood for a 100-year return period event in Guwahati is estimated to be around 1m (Sahoo and Sreeja, 2017), it is assumed that the lowermost 0.5 m and the next 0.5 m of masonry have 20% and 10% strength reduction with respect to the un-weathered masonry, respectively, following an experimental study on masonry infills in timber frames subjected to cycles of weathering and flooding (Stephenson and D'Ayala, 2019). An incremental flood depth analysis (Jalayer *et al.*, 2016) is carried out by monitoring the lateral deflection of the loaded wall panels with each increment of floodwater height, similar to an incremental ground acceleration analysis in the case of seismic loading. The depth of water causing separation of significant parts of the masonry walls is considered as the critical water depth. Closely after reaching the critical depth, the ELS analysis run is terminated when the links representing the mortar cohesion fail and the blocks separate, as it leads to the loss of equilibrium and instability of the problem due to local collapse of the wall.

The lateral out-of-plane deflection vs water depth as obtained from the flood capacity analyses for the un-weathered and weathered models are presented in Figure 3. Appreciable deviation from linear behaviour is found above 0.5m and 1.5m for PD and MD models respectively, where the open cracks started developing in the mortar joints at the base of the long walls. Un-weathered models show an elastoplastic (EP) behaviour until the out-of-plane (OOP) deflection reaches about 15mm. However, in the weathered models, weakening of the lower courses of the masonry limits the elastoplastic capacity to a shorter region. Water heights above the elastoplastic range results in the separation of elements, which causes a sudden drop in the OOP stiffness, in agreement with the experimental observation by Herbert et al. (2012). The ultimate failure of the walls is defined at 60mm deformation (1.71 % drift) as it indicates an OOP failure of the walls (Doherty *et al.*, 2002). Beyond the elastoplastic region, the ultimate failure is very quick, and the pre-cracking and post-cracking phases are distinguished by less than a 100mm increment of water.

Values of the critical depth and EP range are summarised in Table 1, which shows up to 15% and 26% improvement in the flood capacity of the medium design model, as compared to the poor design model, under un-weathered and weathered conditions, respectively. The minimum critical depth value is 1.5m in the case of weathered PD model, which is in the range of the failing flood depths of URM walls (Kelman and Spence (2003); Herbert et al. (2012b); Herbert (2013)). Average hydrostatic pressure corresponding to the critical depths range between 7.35 and 10.79kN/m^2, which is also in agreement with experimental references, for walls in stretcher bond.

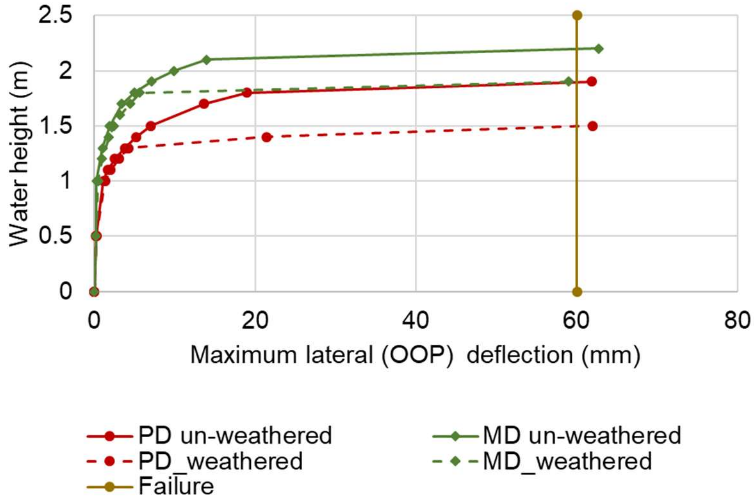

Figure 3. Flood capacity curves for PD and MD models

Table 1. Elastoplastic range and critical depth of water

	Un-weathered			Weathered		
	EP range (m)	h_c (m)	% increase relative to PD	EP range (m)	h_c (m)	% increase relative to PD
PD	1.2-1.7	1.9		1.1-1.3	1.5	
MD	1.5-2.1	2.2	15.79%	1.4-1.8	1.9	26.67%

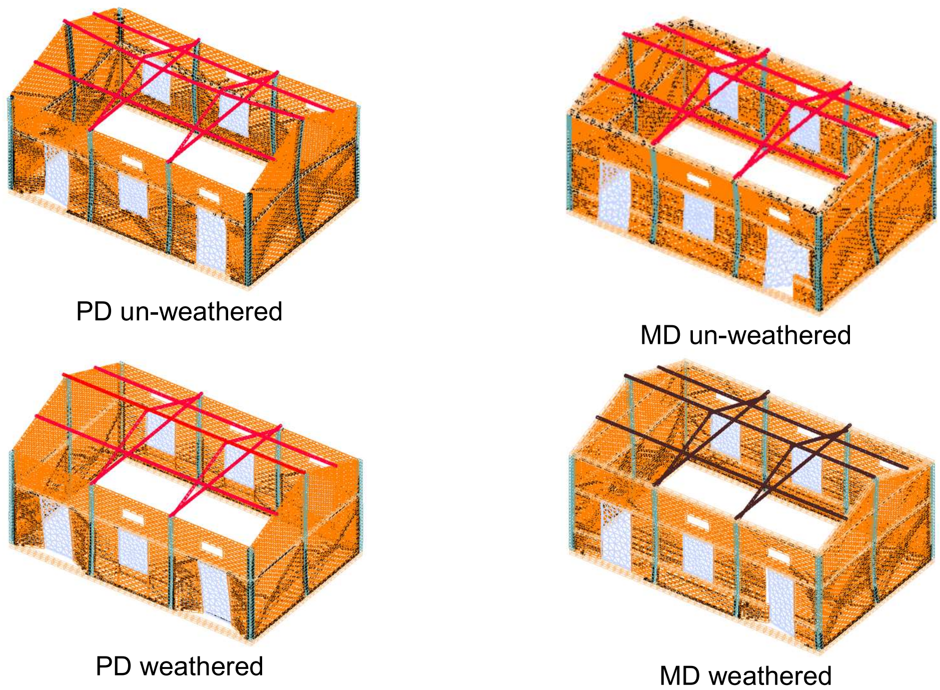

Figure 4. Crack patterns at critical flood depth (exaggerated deflections x10 times, Black marks indicate cracks)

Figure 4 illustrates the typical pattern of cracking on PD and MD models. In all cases, the failure is governed by local failure of wall panels with door openings, with a more pronounced premature failure observed in the weathered models. The flood analysis shows that both PD and MD models do not suffer significant deformation and structural damage at the maximum hazard level identified at the case study location, i.e. 1.00 m water depth.

Combined flood-seismic fragility assessment

The loading scheme shown in Figure 1 is used to account for the material degradation and the combined effects of the floods followed by a seismic action, as discussed previously. In this analysis, the weathered building model is exposed to specified flood depths ranging from 0 to 1 m, in accordance with the hazard characterization of Guwahati. Application of monotonous GA in the transverse direction, after each flood loading event results in distinct capacity curves, each corresponding to that particular sequence of loading (Figure 5a).

As shown in Figure 5a, the combined loading condition reduces the strength and deformation capacity of the models. As compared to 'no flood' case, the strength capacity reduces up to 17.5% and 26% for the PD and MD models, respectively, when the maximum flood depth of 1m is applied. There is significant reduction in ductility of MD model and stiffness of PD model, when the flood depth is increased from zero to 1m. Figure 5b shows the crack patterns at failure, which indicate that the additional design elements such as better confinement present in MD model, while being beneficial in improving its strength capacity by 35%, introduces a discontinuity at sill level causing localised failure, which affects the global ductility by up to 36% with increasing flood depths. Nonetheless the overall capacity of MD is greatly improved with respect to the PD model under the same circumstances.

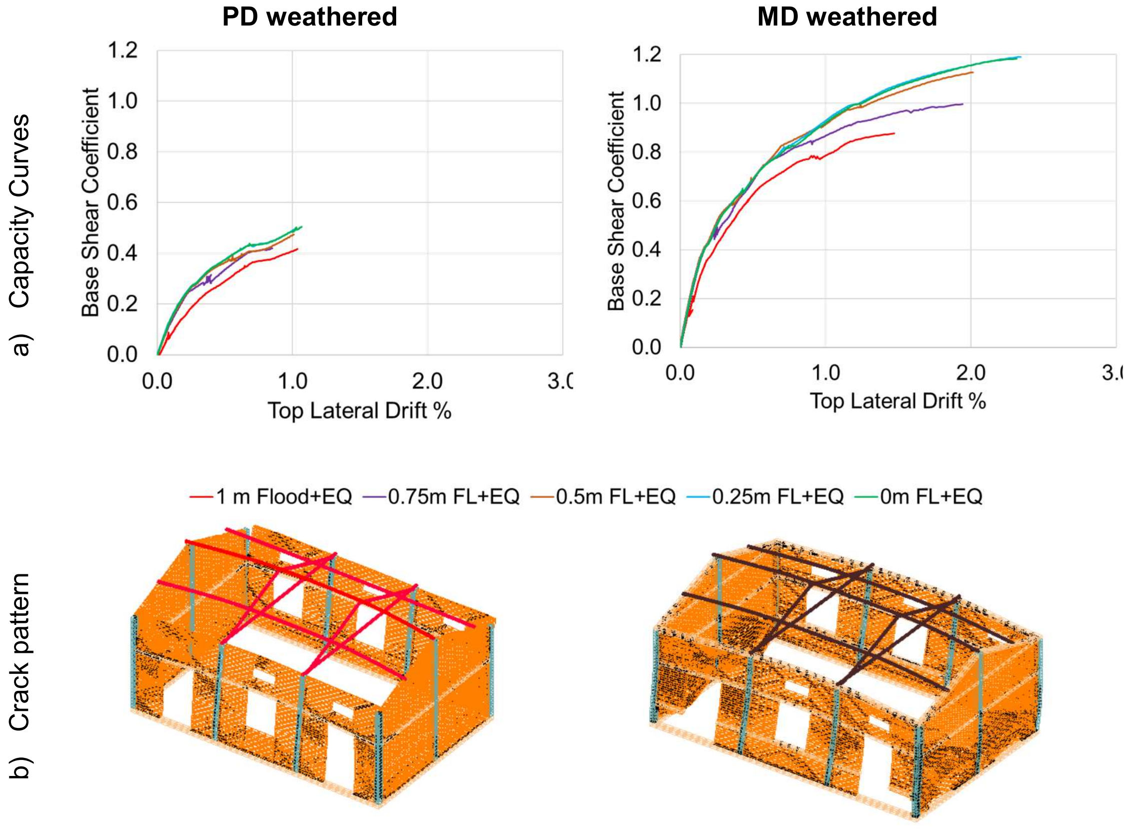

Figure 5. Combined flood-seismic capacity curves

Fragility functions:

The capacity curves shown in Figure 5a, are idealised to bilinear curves and fragility curves are derived using PGA as seismic intensity measure (IM), following the procedure based on nonlinear static analysis and N2 method, as suggested by the Global Earthquake Model guidelines (D'Ayala *et al.*, 2015). In order to derive fragility functions without being specific to the site seismicity, the response spectra of the far-field ground motion records suite provided by FEMA P 695 (FEMA_P695, 2009) is used in this study with scaling, thereby including record-to-record variability. This suit of records are also verified to be suitable for the site seismicity at Guwahati, especially in the range of fundamental periods of the two buildings considered. Least square regression technique is then utilised to derive the lognormal fragility parameters from the cloud of

IM-EDP points. More details of the procedure for the application of N2 method (Fajfar, 2000) for such derivation, are presented in Parammal Vatteri and D’Ayala (2021) and (Parammal Vatteri *et al.*, 2022).

Three damage state thresholds are considered for the fragility derivation, namely, immediate occupancy (IO), life safety (LS) and collapse prevention (CP). These limits are identified differently for the two models. Due to poor connections and minimal confinement, the PD model exhibits a very local OOP overturning failure of the wall above lintel, without mobilising much of the remaining wall capacity. Hence, the performance thresholds are defined according to the progression of cracks and local overturning of the walls. On the other hand, in MD model, IO is identified by cracking initiation in the out-of-plane piers and at the bottom of all walls. Cracks then propagate to spandrels of the OOP walls and diagonal cracks start appearing in the in-plane gable walls, at which stage the LS threshold is reached. Even though the OOP walls suffer local separation of masonry elements at the bottom of the wall, the building withstands further lateral load while maintaining stability until the CP threshold, beyond which large deformations occur for small increment of loads. At this point, the cracks are spread all over the OOP walls and the lower portion of IP walls, although continuous cracks are limited by the presence of RC confining elements. The results of the fragility analysis are presented in Figure 6 and the fragility parameters are listed in Table 2.

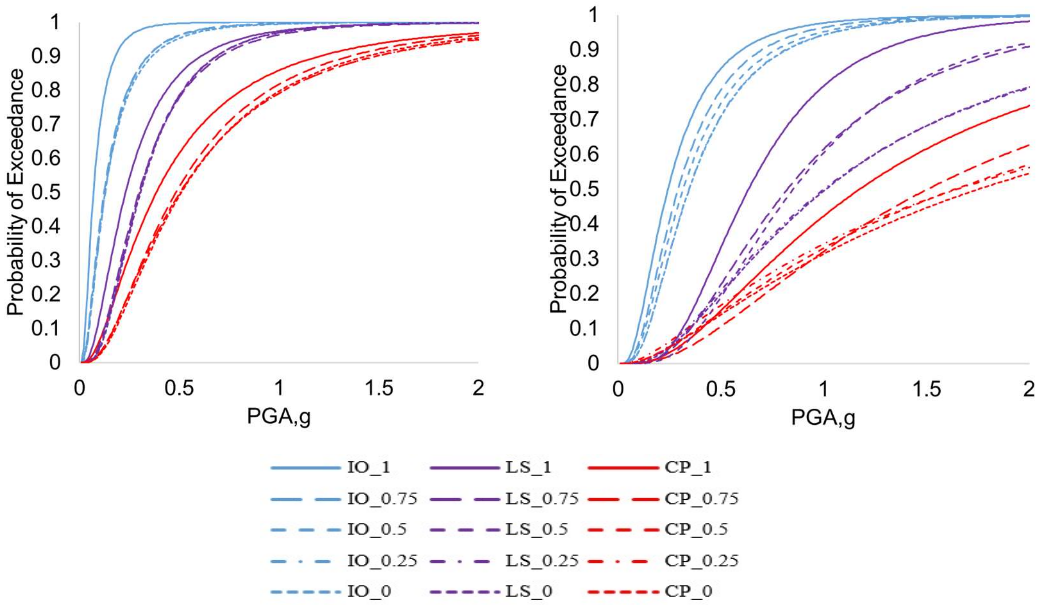

Figure 6. Fragility curves for sequential loading scenario

Table 2 Fragility parameters

Performance levels	**Median PGA of fragility curves corresponding to Flood depths (m)**					**Range of dispersion β**
	1	**0.75**	**0.5**	**0.25**	**0**	
			PD weathered			
IO	0.070	0.123	0.128	0.128	0.128	0.732-0.815
LS	0.231	0.297	0.301	0.301	0.305	0.633-0.754
CP	0.385	0.483	0.503	0.503	0.510	0.804-0.888
			MD weathered			
IO	0.242	0.291	0.316	0.344	0.345	0.672-0.711
LS	0.635	0.823	0.851	1.001	1.010	0.549-0.858
CP	1.175	1.505	1.639	1.647	1.753	0.830-1.236

Conclusions

In order to address the need for multi-hazard assessment methods considering the hazard interaction, a unique loading scheme was developed for combined flood-seismic hazard scenario, which accounts for the recurring and sequential nature of demand arising from the geographic co-existence of these hazards. The two-dimensional fragility functions derived from the numerical analysis characterise the physical fragility of the non-engineered confined masonry buildings with respect to both the hazard intensities. On an average, 18-33% increase is observed in the median PGA values, between the 'no flood' and 'maximum flood' cases in combination with the seismic action, illustrating the significance of the combined hazard effect on the fragility functions.

The study also addressed the need for reliable physical modelling of flood effects on buildings. However, the results of the flood capacity and sequential flood-seismic fragility are dependent on the availability of reliable material degradation data. While the presented approach of sequential loading is well suited for building-level analysis, it is expensive for fragility assessment at regional scale. However, as a next step, this can be achieved by finding a trade-off between the computational expense and the resolution of the fragility functions along the flood intensity axis, for analysing representative buildings from a portfolio. The fragility functions can be further improved by considering the spacial distribution of the flood hazard in the region, and tailoring the sequential analysis for the specific inventory locations.

References

Adhikari, R.K., Parammal Vatteri, A. and D'Ayala, D. (2023) 'Seismic performance assessment of low-rise unreinforced and confined brick masonry school buildings using the Applied Element Method', *Buildings*, 13(1). Available at: https://doi.org/10.3390/buildings13010159.

De Angeli, S. *et al.* (2022) 'A multi-hazard framework for spatial-temporal impact analysis', *International Journal of Disaster Risk Reduction*, 73(January), p. 102829. Available at: https://doi.org/10.1016/j.ijdrr.2022.102829.

ASI (2018) 'Extreme Loading for Structures, Applied Science International, LLC.' North Carolina, USA.: Applied Science International, LLC.

D'Ayala, D.F. *et al.* (2016) 'Assessment of the multi-hazard vulnerability of priority cultural heritage structures in the Philippines', in *ICONHIC*. Chania, Greece.

Bruneau, M. *et al.* (2017) 'State of the Art of Multihazard Design', *Journal of Structural Engineering*, 143(10), p. 03117002. Available at: https://doi.org/10.1061/(asce)st.1943-541x.0001893.

Calvi, G.M. *et al.* (2006) 'Development of seismic vulnerability assessment methodologies over the past 30 years', *ISET Journal of Earthquake Technology*, 43(3), pp. 75–104.

D'Ayala, D. *et al.* (2015) *Guidelines for Analytical Vulnerability Assessment - Low / Mid-Rise*. Global Earthquake Model. Available at: https://doi.org/10.13140/RG.2.1.1893.1609.

D'Ayala, D., Copping, A. and Wang, H. (2006) 'A Conceptual Model for Multi-Hazard Assessment of the Vulnerability of Historic Buildings', in *Structural Analysis of Historical Constructions: Possibilities of Numerical and Experimental Techniques, Proceedings of the Fifth International Conference, New Delhi, India.*

Dabbeek, J. *et al.* (2020) 'Probabilistic earthquake and flood loss assessment in the Middle East', *International Journal of Disaster Risk Reduction* [Preprint]. Available at: https://doi.org/10.1016/j.ijdrr.2020.101662.

Doherty, K. *et al.* (2002) 'Displacement-based seismic analysis for out-of-plane bending of unreinforced masonry walls', *Earthquake Engng Struct. Dyn*, 31(4), pp. 833–850. Available at: https://doi.org/10.1002/eqe.126.

Fajfar, P. (2000) 'A non-linear analysis method for performance-based seismic design', *Earthquake Spectra*, 16(3), pp. 573–592.

FEMA_P695 (2009) *Quantification of Building Seismic Performance Factors*. Federal Emergency Management Agency (FEMA), American Society of Civil Engineers.

GADRRRES (2022) *Comprehensive School Safety Framework 2022-2030 for Child Rights and Resilience in the Education Sector*.

GADRRRES and UNISDR (2017) *Comprehensive school safety,A global framework in support of The Global Alliance for Disaster Risk Reduction and Resilience in the Education Sector and The Worldwide Initiative for Safe Schools*.

Gallina, V. *et al.* (2016) 'A review of multi-risk methodologies for natural hazards: Consequences and challenges for a climate change impact assessment.', *Journal of Environmental Management*, 168, pp. 123–132.

Gehl, P. (2017) *Bayesian Networks for the Multi-Risk Assessment of Road Infrastructure (Thesis)*. University College London, UK.

GPSS (2014) *Global Program for Safer Schools*, *The World Bank*. Available at: https://gpss.worldbank.org/.

Herbert, D.M. *et al.* (2012) 'The strength of masonry walls when subject to flood loading', in *15th International Brick and Block Masonry Conference*.

Herbert, D.M. (2013) *An investigation of the strength of brickwork walls when subject to flood loading (Thesis)*. Cardiff University.

ISDR (2005) *Hyogo framework for action 2005–2015: Building the Resilience of Nations and Communities to Disasters*, *World Conference on Disaster Reduction*. Available at: https://doi.org/10.1007/978-1-4020-4399-4_180.

Jalayer, F. *et al.* (2016) 'Performance-based flood safety-checking for non-engineered masonry structures', *Engineering Structures*, 106, pp. 109–123. Available at: https://doi.org/10.1016/j.engstruct.2015.10.007.

Kelman, I. and Spence, R. (2003) 'A limit analysis of unreinforced masonry failing under flood water pressure', *Masonry International*, pp. 51–61.

Marzocchi, W. *et al.* (2012) 'Basic principles of multi-risk assessment: a case study in Italy', *Natural Hazards*, 62(2), pp. 551–573.

Mendis, W., De-Silva, S. and De-Silva, G.S. (2014) 'Performance and Retrofitting of Unreinforced Masonry Buildings against Natural Disasters–A Review Study', *Engineer: Journal of The Institution of Engineeers Sri Lanka* [Preprint], (February). Available at: https://doi.org/10.4038/engineer.v47i3.6896.

Murnane, R.J. *et al.* (2017) 'Future scenarios for earthquake and flood risk in Eastern Europe and Central Asia', *Earth's Future*, 5(7), pp. 693–714. Available at: https://doi.org/10.1002/2016EF000481.

Nofal, O.M. and van de Lindt, J.W. (2020) 'Minimal building flood fragility and loss function portfolio for resilience analysis at the community level', *Water (Switzerland)*, 12(8). Available at: https://doi.org/10.3390/w12082277.

Parammal Vatteri, A. and D'Ayala, D. (2021) 'Classification and seismic fragility assessment of confined masonry school buildings', *Bulletin of Earthquake Engineering* [Preprint], (0123456789). Available at: https://doi.org/10.1007/s10518-021-01061-9.

Parammal Vatteri, A., D'Ayala, D. and Gehl, P. (2022) 'Bayesian networks for the assessment of disruption to school systems under combined hazards', *International Journal of Disaster Risk Reduction*, 74. Available at: https://doi.org/https://doi.org/10.1016/j.ijdrr.2022.102924.

Putrino, V. (2021) *Multi-Hazard Vulnerability Assessment of Unreinforced Masonry Structures*. University College London.

Ritchie, H. and Roser, M. (2014) *Natural Disasters*, *OurWorldInData.org*. Available at: https://ourworldindata.org/natural-disasters (Accessed: 20 January 2020).

Rossetto, T. and Elnashai, A. (2003) 'Derivation of vulnerability functions for European-type RC structures based on observational data', *Engineering Structures*, 25, pp. 1241–1263.

Roy, T. and Matsagar, V. (2021) 'Multi-hazard analysis and design of structures: status and research trends', *Structure and Infrastructure Engineering*, 19(6), pp. 845–874. Available at: https://doi.org/10.1080/15732479.2021.1987481.

de Ruiter, M.C. *et al.* (2017) 'Review Article : A Comparison of Flood and Earthquake Vulnerability Assessment Indicators', *Nat. Hazards Earth Syst. Sci.*, pp. 1–34. Available at:

https://doi.org/10.5194/nhess-2017-45.

de Ruiter, M.C., de Bruijn, J.A., *et al.* (2020) 'The asynergies of structural disaster risk reduction Measures: comparing floods and earthquakes', *Earth's Future* [Preprint]. Available at: https://doi.org/10.1029/2020EF001531.

de Ruiter, M.C., Couasnon, A., *et al.* (2020) 'Why we can no longer ignore consecutive disasters', *Earth's Future*, 8. Available at: https://doi.org/10.1029/2019EF001425.

Sahoo, S.N. and Sreeja, P. (2017) 'Development of Flood Inundation Maps and Quantification of Flood Risk in an Urban Catchment of Brahmaputra River', *ASCE-ASME J. Risk Uncertainty Eng. Syst., Part A: Civ. Eng.*, 3(1), pp. 1–11. Available at: https://doi.org/10.1061/AJRUA6.0000822.

Shah, A.A. *et al.* (2018) 'Living with earthquake and flood hazards in Jammu and Kashmir, NW Himalaya', *Frontiers in Earth Science*, 6(November), pp. 1–13. Available at: https://doi.org/10.3389/feart.2018.00179.

Stephenson, V. and D'Ayala, D. (2019) 'Structural Response of Masonry Infilled Timber Frames to Flood and Wind Driven Rain Exposure', *Journal of Performance of Constructed Facilities*, 33(3). Available at: https://doi.org/10.1061/(ASCE)CF.1943-5509.0001281.

The World Bank (2019) *Global Library of School Infrastructure (GLOSI), Global Program for Safer Schools (GPSS)*. Available at: https://gpss.worldbank.org/en/glosi (Accessed: 5 December 2019).

UN (2002) *Plan of Implementation of the World Summit on Sustainable Development Contents*, *Johaneesburg plan of implementation*.

UNISDR (2015) *Sendai Framework for Disaster Risk Reduction 2015 - 2030*, *rr.org/uploads/Sendai_Framework_for_*. Available at: http://www.wcdrr.org/uploads/Sendai_Framework_for_Disaster_Risk_Reduction_2015-2030.pdf.